# Material behaviour of austenitic stainless steel subjected to cyclic and arbitrary strain loading

Lucy Lázaro, Rolando Chacón
School of Civil Engineering
Department of Civil and Environmental Engineering
Universitat Politècnica de Catalunya

## Abstract

In this paper, an experimental program on cyclic loading of austenitic stainless steel specimens is presented. The program encompasses a series of forty specimens subjected both cyclic (low and extremely low) and arbitrary loading (following certain rules). These protocols include companion, multiple-step and a set of arbitrary earthquake-like strain history, which represents a novelty in the material understanding. Stainless steel exhibits strain hardening as a key feature for structural applications. This feature is fundamental in the definition of cross-sectional resistance, cross-section classification, ductility and energy dissipation. In recent years, the strategic use of stainless steel as a potential structural material in dissipative zones of earthquake-resistant elements is under consideration. When it comes to seismic design, strain-hardening must be known precisely for further characterization of the seismic structural behaviour of the actual system in which stainless steel is used strategically. The use of stainless steel in dissipative zones of earthquake-resistant structures requires research related to cyclic loading at many levels. Thus, its potential use in seismic areas, as well as the performance of existing structures, can be considered. A systematic analysis of the results, which include cyclic hardening, stabilization and material degradation, is presented. In addition, these results are used for the further numerical implementation of cyclic hardening in non-linear models.

## 1. Introduction

The use of stainless steel in structures has increased in recent years due to its unique combination of mechanical properties, durability and aesthetics. Stainless steel is a metallic alloy whose usage increases in the construction industry. Its corrosion resistance, coupled with relatively high strength and ductility, makes stainless steel particularly appealing for its structural use in highly aggressive and corrosive environments. The chromium content provides beneficial effects when it comes to corrosion resistance but also modifies the mechanical behavior, resulting in a metallic alloy with a non-linear stress-strain response that has to be accounted for adequately at all stages of structural design. In particular, since cyclic hardening has been observed experimentally in these alloys, the potential use of stainless steel in dissipative zones of earthquake-resistant structures needs to be studied in detail for structural applications.

In recent decades, several studies related to material non-linearity under monotonic incremental loading have been published [1]–[3]. When it comes to corrosion and durability, studies have also been published in recent years [4]–[6]. In the case of structural applications, a new generation of research projects aimed at studying stainless steel structures and the effects of the material non-linearity on the global behaviour of frames is nowadays active [7]–[14]. Other studies are focusing on the use of stainless steel on dissipative zones only (zones in which plastic strain is concentrated) as part of a more strategic use of the material [9][15][16]. In any case, stainless steel frames may provide a relatively different response when compared to carbon steel frames when subjected to arbitrary reversal loading with severe plastic strains as found in typical seismic episodes.

As a result, characterization of the material is a paramount task for a further adequate modelling of the aforementioned cyclic characteristics. The characterisation includes defining cyclic hardening, stabilisation and degradation of the material while loading cyclically. In this paper, an experimental program on stainless steel elements subjected to cyclic loading is presented. The main objective of this research consists of providing experimental data to the research community together with contributing to the understanding of the cyclic behaviour and low-cycle fatigue of grade EN 1.4307 austenitic stainless steel when intended for dissipative

zones. The experimental program encompasses a set of forty specimens tested under different protocols. The tests performed were low-cycle fatigue tests at strain amplitudes ranging from ±0.5% to ±5% and include several standard protocols such as companion and multiple steps but also, a set of arbitrary loading protocols that are aimed at understanding the effect of the loading history on the material. Experimental observations show that austenitic stainless steel under cyclic loading with relatively high plastic strain presents considerable hardening and a noticeable stabilisation after a certain number of cycles. From the performed tests, analytical parameters necessary for the implementation of further numerical models are extracted. Finally, experimental observations related to the effect of the loading history on stainless steel subjected to cyclic loading are provided.

## 2. Review of earlier work.

### 2.1. Analytical model

Early studies on low cycle fatigue in stainless steel found a significant feature, strain hardening. Most of these studies used the Chaboche model [17] to characterise its behaviour, which includes strain hardening and the Bauschinger effect.

Non-linear numerical models in which the Chaboche model is used are based on the following definitions:

Isotropic hardening, which defines the increase of yield surface size ($\sigma^0$), is given as Eq.(1):

$$\sigma^0 = \sigma|_0 + Q_\infty\left(1 - e^{-b\varepsilon^p}\right) \tag{1}$$

where $\sigma|_0$ is initial yielding stress when plastic strain equals zero, $Q_\infty$ is the maximum change in the size of the yield surface, $\varepsilon^p$ is plastic strain, and $b$ is the parameter that defines the rate at which the size of the yield surface changes as plastic strain increases. For obtaining $Q_\infty$ and $b$ experimental data in the form $(\sigma_i^0, \varepsilon_i^p)$ for each $i$ cycle is needed.

The size of the yield surface $\sigma_i^0$ and the plastic strain $\varepsilon_i^p$ in the arbitrary cycle i are defined as Eq. (2) and (3).

$$\sigma_i^0 = (\sigma_i^t - \sigma_i^c)/2 \tag{2}$$

$$\varepsilon_i^p = \frac{1}{2}(4i - 3)\Delta\varepsilon^p \tag{3}$$

$$\Delta\varepsilon^p \approx \Delta\varepsilon - 2\sigma_1^t/E \tag{4}$$

where $\sigma_i^t$ is the maximum tensile stress, $\sigma_i^c$ is the maximum compressive stress, and $\Delta\varepsilon^p$ is the total plastic strain as Eq. 4

On the other hand, for a defined backstress $\alpha$, kinematic hardening is defined as Eq. (5). Backstress refers to the stress coordinate of the middle point between the yield stress in tension and compression.

$$\alpha = \frac{C_k}{\gamma_k}\left(1 - e^{-\gamma\varepsilon^p}\right) + \alpha_1 e^{-\gamma\varepsilon^p} \tag{5}$$

where $C_k$ is the initial kinematic hardening modulus and $\gamma_k$ is the rate at which the kinematic hardening modulus decreases with increasing plastic deformation.

Again, the values of pair $(\sigma_i^0, \varepsilon_i^p)$ data are obtained from test data. $\varepsilon_i^p$ is the plastic strain in the cycle i and defined as Eq. (6)

$$\varepsilon_i^p = \varepsilon_i - \frac{\sigma_i}{E} - \varepsilon_p^0 \tag{6}$$

where $\varepsilon_p^0$ is the strain when the curves intercept with the strain axis, the strain initial is zero $\varepsilon_i^p = 0$. The backstress can be obtained according to Eq. (7)

$$\alpha_i = \sigma_i - \sigma^s \quad (7)$$

where $\sigma^s$ is the average of the first and last data points stress in a stabilised loop. When the tests reach a steady-state condition, a stabilised loop is considered.

The values required to fit the curves and the parameters are obtained from a stabilised hysteresis loop from cyclic test data. Therefore, cyclic test data in the $\sigma, \varepsilon$ form are necessary in order to use the Chaboche model.

## 2.2. Experimental Studies

The study of low and extremely low cycle fatigue in metals is widely developed by various authors [18]–[21]. In steels, a complete methodology to study the monotonic and cyclic test data of smooth geometries is detailed in [22], which could be used in other metals such as stainless steel.

Experimental studies which used stainless steel specimens subjected to cyclic loading with several protocols are found. These studies characterise the cyclic behaviour of stainless steel with high accuracy on test data and determined the parameters of isotropic and kinematic hardening for the Chaboche model. Table 1 illustrates these parameters as well as the researchers that describe them, where the numbers in bold represent the average results. The values of isotropic and kinematic hardening show scattering, which can be affected by factors such as the grade of stainless steel and strain amplitude.

Table 1: Parameters of isotropic and kinematic hardening from previous studies

| **Reference** | **Strain amplitudes (%)** | **Isotropic hardening** | | | **Kinematic hardening** | |
|---|---|---|---|---|---|---|
| | | $\sigma\|_0$ (MPA) | $Q_\infty$ (MPA) | **B** | **Ck** (MPA) | **γk** |
| K.H. Nip et al.[23] | ±1% | **225** | **432** | **0.16** | **175450** | **421** |
| | ±3% | **237** | **517** | **1.17** | **82675** | **186** |
| | ±5% | **246** | **418** | **2.16** | **88520** | **180** |
| | ±7% | **225** | **594** | **1.76** | **125600** | **216** |
| A. Dutta et al.[24] | ±0,6% | 225 | 60 | 9.71 | 42096 | 595 |
| S. Chandra et al.[25] | ±0,5% | 211 | 42 | 21.60 | 57805 | 619 |
| Y.Q. Wang et al.[26] | ±0,4% | 234 | 77 | 10.50 | 56760 | 420 |
| Chacón et al.[27] | ±3.0% | 319 | 327 | 0.66 | 33396 | 163 |
| | ±5.0% | | 156 | 3.14 | 67381 | 206 |
| X. Chang et al.[28] | max. +1.5% | 299 | 62 | 6.60 | 65020 | 662 |
| | | | | | 41222 | 417 |
| | | | | | 31286 | 319 |
| | | | | | 23210 | 249 |
| Baiguera et al.[29] | max. 0.8dy (*) | 400 | 200 | 5.00 | 6500 | 30 |
| | | | | | 100000 | 700 |
| F. Yin et al.[30] | max. +1.5% | 171 | 81 | 15.10 | 18263 | 224 |
| | | | | | 15524 | 188 |
| | | | | | 13774 | 163 |
| | | | | | 11633 | 138 |
| A. Charles-Darwin et al.[31] | ±1%, ±2% | 116 | 157 | 1.50 | 100000 | 2000 |
| | | | | | 80000 | 1500 |
| | | | | | 40000 | 1000 |
| | | | | | 15000 | 300 |
| | | | | | 9450 | 101 |

(*) dy stands for yield displacement

Table 2: Material, Loading protocol, Strain rates in previous experimental studies

| Reference | Stainless steel type | Test method | Strain rate ($s^{-1}$) |
|---|---|---|---|
| K.H. Nip et al.[23] | EN 1.4301 and 1.4307 | Companion | $5x10^{-3}$ |
| A. Dutta et al.[24] | EN 1.4401 | Companion | $1x10^{-3}$ |
| S. Chandra et al.[25] | EN 1.4404 | Companion | $3x10^{-3}$ |
| Y.Q. Wang et al.[26] | EN 1.4401 | Companion and multiple step | 0.05 Hz |
| Chacón et al.[27] | EN 1.4301 | Companion | $1x10^{-3}$ |
| X. Chang et al.[28] | S220503 (AISI) | Companion, multiple step, descendant test | - |
| Baiguera et al.[29] | S31803 F51 (AISI) | Multiple step | 1mm/min |
| F. Yin et al.[30] | S30408 (AISI) | Companion, multiple step, descendant test | - |
| A. Charles-Darwin et al.[31] | 304L (AISI) | Multiple step (AISC protocol [32]) | $1x10^{-3}$ |

Table 2 depicts the type of stainless steel studied, the method of test used and the strain rate of the tests. The material type was austenitic and duplex stainless steel due to their advantage in ductility and strength. The methods employed to carry out the aforementioned tests were: companion method [33], multiple step [33], and in some cases, an arbitrary protocol.

Concerning these arbitrary protocols, Xie et al. [34] studied 14 ascending/descending and 3 random cyclic loading tests of low alloy structural steel and found the conventional Chaboche model could not predict accurately the cyclic behaviour of this material under irregular loading protocol, thus developing a new constitutive model based on the multi-surface model.

As for the multi-surface model, Chang et al. [28], Baiguera et al.[29], Yin et al.[30], and Annan et al.[31] used a yield surface and more than one backstress with appropriate accuracy on the tests data. In this case, they developed a unique numerical model with these features.

On the other hand, Nip et al.[23] and Chacón et al.[27] showed a value of yield surface and backstress for each strain amplitude. Therefore, they developed several numerical models of stainless steel.

Another important aspect is the strain rate at which tests were carried out, which had a range of $1 \times 10^{-3}$ $s^{-1}$ ([24],[27] and [31]), $3 \times 10^{-3}$ $s^{-1}$ ([35] and [25]) and $5 \times 10^{-3}$ $s^{-1}$ [23] to discard overheating in the specimen during the tests. Nevertheless, the seismic events occur in very short periods, i.e. very fast.

S. Jia et al.[36] studied the difference between low, medium ($10^{0}$-$10^{2}$ $s^{-1}$) and high strain rates ($10^{2}$-$10^{4}$ $s^{-1}$) in stress-strain curves of austenitic stainless steel and found yield and ultimate strength increased with a strain rate ranging from $1 \times 10^{-3}$ $s^{-1}$ to $1 \times 10^{4}$ $s^{-1}$. Therefore, the material proved to be stronger as the strain rate increased.

As mentioned before, in this study we used a strain rate of $1 \times 10^{-3}$ $s^{-1}$ to prevent constant strain amplitudes protocols from overheating and an additional test with a strain rate of $1 \times 10^{-2}$ $s^{-1}$ for arbitrary protocols to assess the strength variation in function of the strain rate.

## 3. Experimental program

A set of tests of 40 specimens under different types of cyclic loading was carried out. The material studied was austenitic stainless steel EN 1.4307, whose composition can be seen in table 3. The specimens were smooth bars with a geometric design according to ASTM (2012) E606/E606M [37] as figure 1 illustrates.

Table 3: Composition of austenitic stainless steel EN. 1.4307

| %C | % Si | % Mn | % P | % S | % Cr | % Ni | % Mo | N2 PPM | % Cu | % Sn | % Pb |
|---|---|---|---|---|---|---|---|---|---|---|---|
| 0.018 - 0.030 | 0.25 - 0.45 | 1.30 - 1.70 | ≤ 0.40 | 0.022 - 0.030 | 18.00 - 18.30 | 8.00 - 8.20 | ≤ 0.50 | 700 - 900 | ≤ 0.50 | ≤ 0.025 | ≤ 0.0010 |

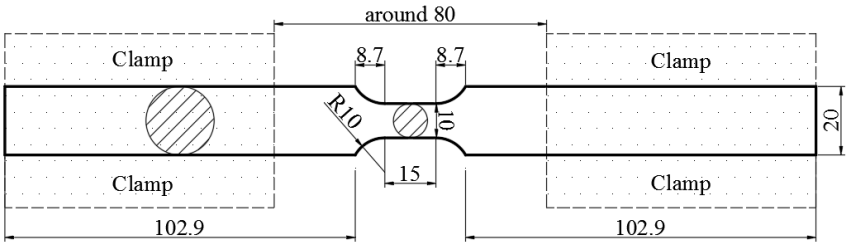


Figure 1: geometries design of specimens (measures are in mm)

### 3.1. Equipment

All tests were carried out at the Structures and Materials Laboratory (LATEM) in the Polytechnic University of Catalonia. In all cases, Instron 8803 [38] was used, which has a servohydraulic fatigue testing system that performs monotonic and cyclic tests and loads and allows to reach loads up to 500 kN. Figure 2(a) shows the main components of Instron 8803. There is a distance between inner clamps of approximately 80mm. This distance was calculated using models of elastic buckling of pieces subjected to the maximum expected compressive strain (≈ ±5%).

To input data, Instron 8803 uses a console named WaveMaker, a graphical user interface software that operates by entering data through blocks, which can be seen in figure 2(b).

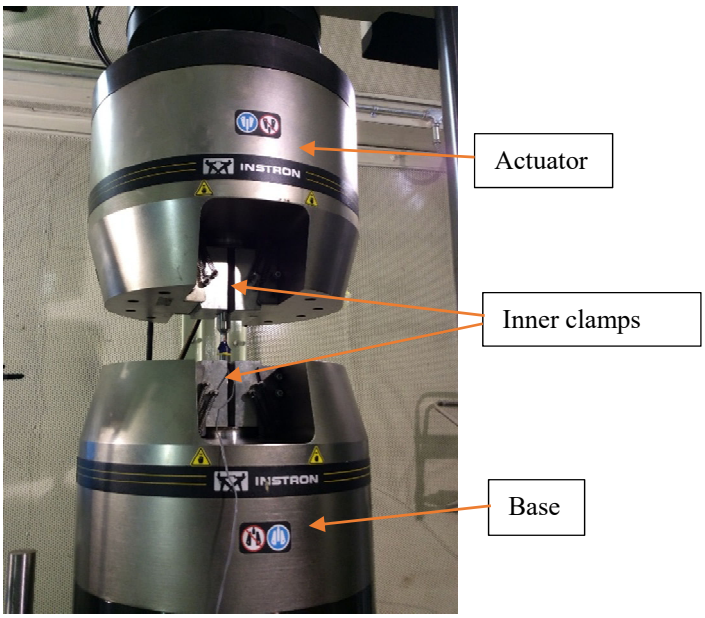


(a)

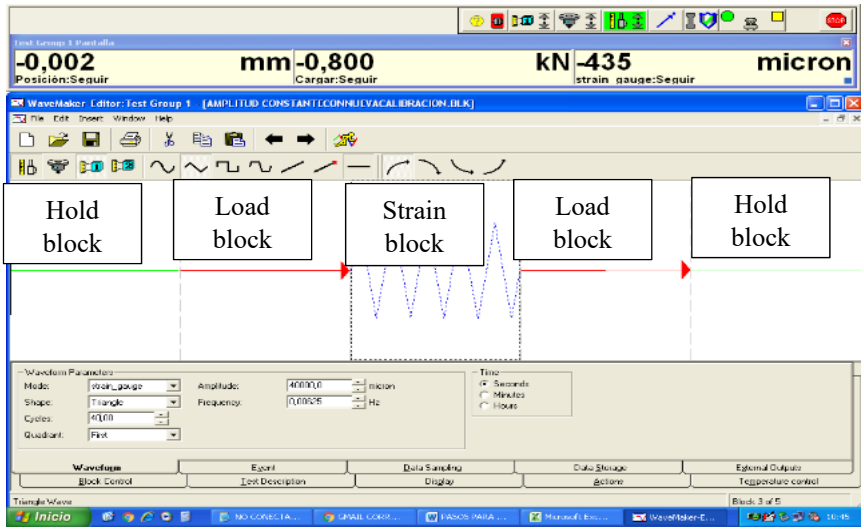


(b)

Figure 2: (a) Instron 8803, (b) Console WaveMaker

Two instruments were used to control the tests: the first one was a 3mm long strain gauge with the following features: type FLAB-3-17-3LJC-F [39], 2.11 as a gauge factor, and two terminals, which can be seen in figure 3(a). The second instrument was an extensometer gauge model 3541-005M-0635M-ST with a gauge length of 5.08mm and a range from -1.27mm to +6.35mm (manufacturer information). As figure 3(b) illustrates, this instrument requires additional clips in order to attach it to the corresponding sample.

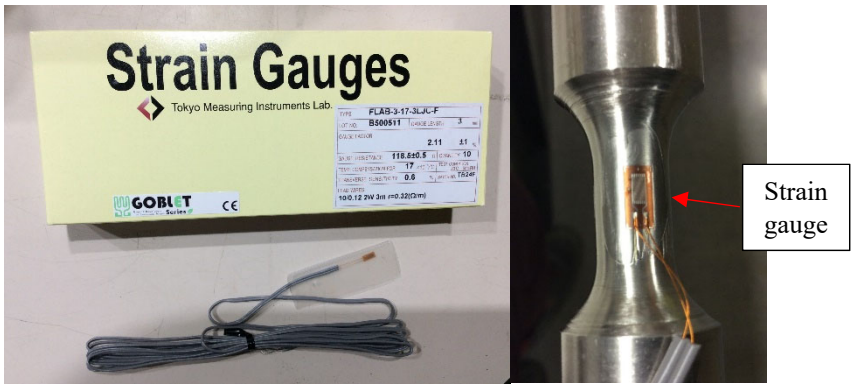


(a)

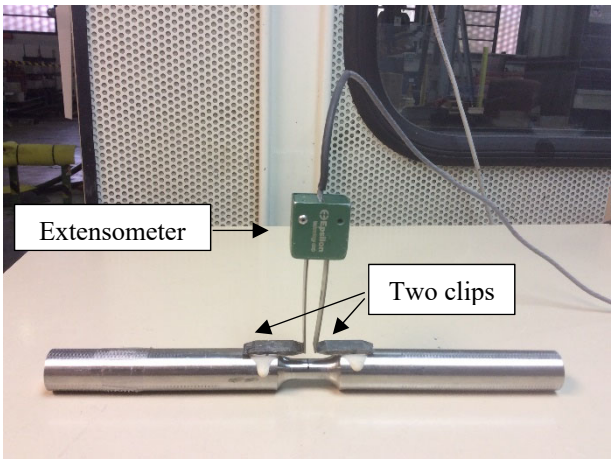


(b)

Figure 3: (a) Strain gauge sensor, (b) extensometer gauge

Adhesives used were cyanoacrylate adhesive for the strain gauge and the specimen. Before applying the adhesives, the surface of the specimens was polished to obtain a certain degree of roughness for warranting adhesion.

It is important to note that in all tests, the main control was through the strain gauge. The test protocol was developed directly by entering the strain value. In some specific cases, the strain gauge malfunctioned. Since an extensometer was installed on the specimen as a redundant measurement and the relationship between strain and displacement was known and calibrated. It represented an extra safety measurement that was used for completing such tests. The number of cycles included those strain-controlled added to the extensometer-controlled (if any).

### 3.2. Types of tests

Four types of tests were carried out: monotonic tests (MT), companion tests (CT), multiple step (MS) tests, and seismic recorder (SR) tests. The specimens were labelled respectively.

The label notations used are specified as follows (figure 4): MT, CT, MS and SR are the type of tests, 0.5 is the ±0.5% of strain amplitude, 10C is the number of cycles of every ascendant block, V1 is the strain rate of 1 x $10^{-3}$ $s^{-1}$, and 1 refers to the number of specimens. There was a different type of seismic recorder test labelled SR-V1-0.5, where 0.5 refers to the ±0.5% pre-established set of strain cycles. Figure 4 shows examples of these notations.

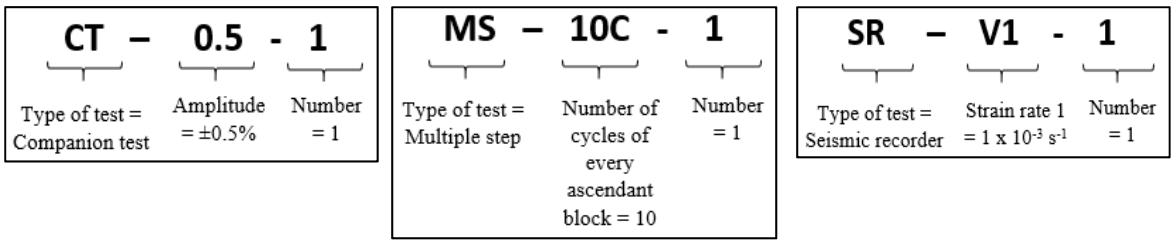


Figure 4: Example of companion test notation

#### 3.2.1. Monotonic test

This test was carried out to obtain the key characteristics of stainless steel, i.e. Young's Modulus, yield strength, etc. and consisted of the application of uniaxial displacement until reaching the fracture of the specimen. The displacement was applied to one end of the specimen whereas the other end was fixed. The control was through the position displacement of Instron 8803, data collection was through an extensometer and a strain gauge placed in the middle of the length with reduced cross-section.

The displacement rate was the one recommended by [40] that consists of 4 stages: (1) elastic range from start to proportional elastic limit, (2) yielding range from proportional elastic limit to yield strength, (3) strain hardening range from yield strength to ultimate strength, and (4) post-ultimate range from ultimate strength to fracture. In this study, a yield strength of 0.2% proof stress was taken and ultimate strength was the maximum strength achieved. Figure 5 shows the values used in each stage.

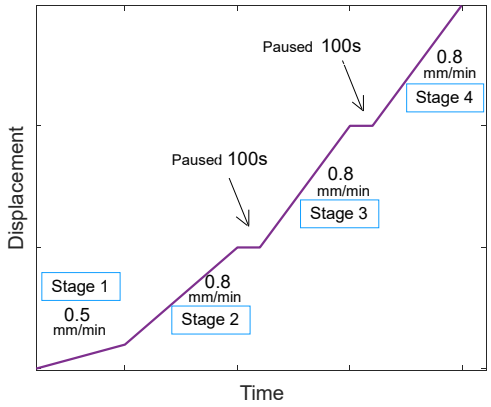


Figure 5: displacement rate in monotonic test

The results obtained from MT-1 were corrected according to [40]. This is depicted in figure 6 as well as the representation of Young's Modulus. Table 4 shows the key properties obtained from output data from the strain gauge in this test.

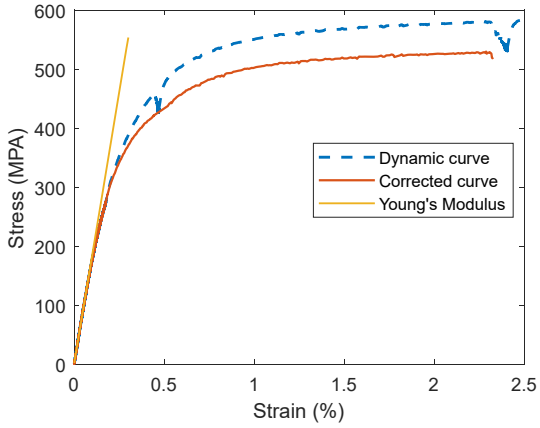


Figure 6: Monotonic strain-stress curve (dynamic and corrected curve)

It is worth mentioning that the dynamic curve showed greater values than the corrected ones due to the pause of 100 seconds performed in the test.

Table 4: Key monotonic properties of stainless steel

| E (N/mm2) | $\sigma_{0.2}$ (N/mm2) | Ey (N/mm2) | n | m |
|---|---|---|---|---|
| 184152.71 | 416.36 | 24113.92 | 6 | 4.4 |

where E is Young's Modulus; $\sigma_{0.2}$ is the yield strength defined herein as the proof stress for a 0.2% offset strain; Ey is the tangent modulus at yield strength; n is a strain hardening exponent and m is a parameter of roundedness. These parameters are used in the Ramberg-Osgood [41], Mirambell and Real [3], and Rasmussen [2] formulations to characterise the stress-strain curve.

### 3.2.2. Companion test

This method is often used to characterise the low cycle fatigue behaviour and consists of the application of cycles of tension and compression with constant amplitude strain in each specimen as shown in figure

7(a). As in the monotonic test, the strain was applied to one end of the specimen whereas the other end was fixed. This methodology was employed in all tests.

A set of 21 specimens for several constant amplitude strains were used. Table 5 summarises the constant amplitude strains in this test. Strain gauges of 3mm were used for the control with a strain rate of 1 x $10^{-3}$ $s^{-1}$ for all tests. All tests were strain-controlled using the strain gauge. In some cases, it malfunctioned at an advanced level of cycles before the specimen failed. Then, the control was performed using an extensometer until the specimen reached failure. The number of cycles considered when studying low cycle fatigue was defined as the total amount of registered cycles (strain-controlled plus extensometer controlled). Tests were performed until they reached fracture of the material or buckling of the specimen.

In some cases, buckling was observed when the specimens reached large values of axial load (compression). The tests were initially designed in such a way the maximum expected compression was lower than the expected buckling load on an ideal specimen. Throughout the cyclic loading, the material was degraded, which also degraded this ideal expected load. In some cases, due to this effect, that load might be achieved. Some authors suggest anti-buckling devices when studying cyclic loading in flat pieces subjected to compression greater than the expected out-of-plane buckling load [22].

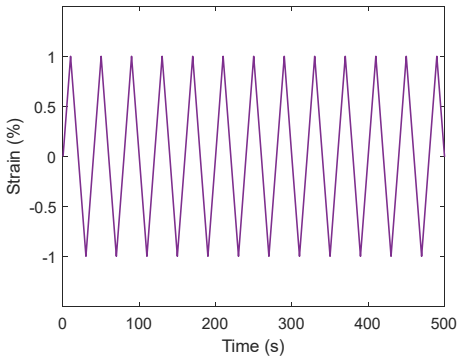


(a) Companion test from 1% strain amplitude

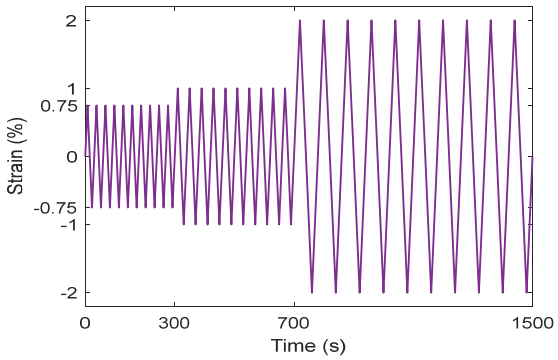


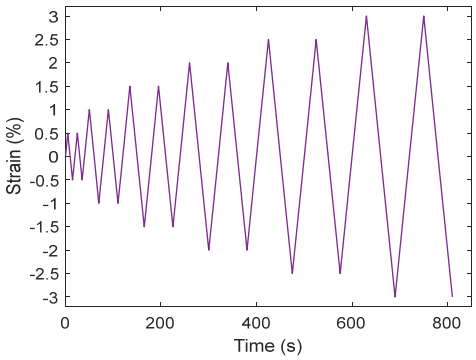


(b) Multiple step test every 10 cycles

(c) Multiple step test every 2 cycles

Figure 7: Load protocol, companion and multiple step test

Table 5: Constant amplitude strain used

| Specimen | Amplitude | Cycles reached with strain gauge | Cycles reached with extensometer | Final state of specimen |
|---|---|---|---|---|
| CT-0.5-1 | ±0.5% | 1735 | 6937 | Fractured |

| | | | | |
|---|---|---|---|---|
| CT-0.5-2 | ±0.5% | 2181 | 4238 | Fractured |
| CT-0.5-3 | ±0.5% | 1887 | --- | Buckling |
| CT-0.75-1 | ±0.75% | 350 | 1869 | Fractured |
| CT-0.75-2 | ±0.75% | 472 | 1285 | Fractured |
| CT-0.75-3 | ±0.75% | 801 | 500 | Fractured |
| CT-1.0-1 | ±1% | 250 | 332 | Fractured |
| CT-1.0-2 | ±1% | 158 | 350 | Fractured |
| CT-1.0-3 | ±1% | 197 | --- | Necking* |
| CT-2.0-1 | ±2.0% | 49 | 70 | Fractured |
| CT-2.0-2 | ±2.0% | 45 | 88 | Fractured |
| CT-2.5-1 | ±2.5% | 24 | 47 | Fractured |
| CT-2.5-2 | ±2.5% | 18 | --- | Buckling |
| CT-3.0-1 | ±3% | 11 | --- | Buckling |
| CT-3.0-2 | ±3% | 10 | 36 | Fractured |
| CT-3.5-1 | ±3.5% | 10 | --- | Fractured* |
| CT-3.5-2 | ±3.5% | 12 | 22 | Fractured |
| CT-4.0-1 | ±4% | 4 | --- | Fractured* |
| CT-4.0-2 | ±4% | 4 | --- | Fractured* |
| CT-5.0-1 | ±5% | 1 | 18 | Fractured |
| CT-5.0-2 | ±5% | 1 | --- | Fractured* |

(*) Necking and fractured due to detachment strain gauge

Figure 8 (a) illustrates the number of cycles reached until the failure of the specimen by each strain amplitude. The failure was considered when the stress decreased 10% of the maximum stress reached in each test. Figure 8(b) improves the visualisation of the number of cycles of strain amplitudes from ±2% to ±5%, because they are less than$10^3$. It is important to note that the considered data from the extensometer only referred to the number of cycles.

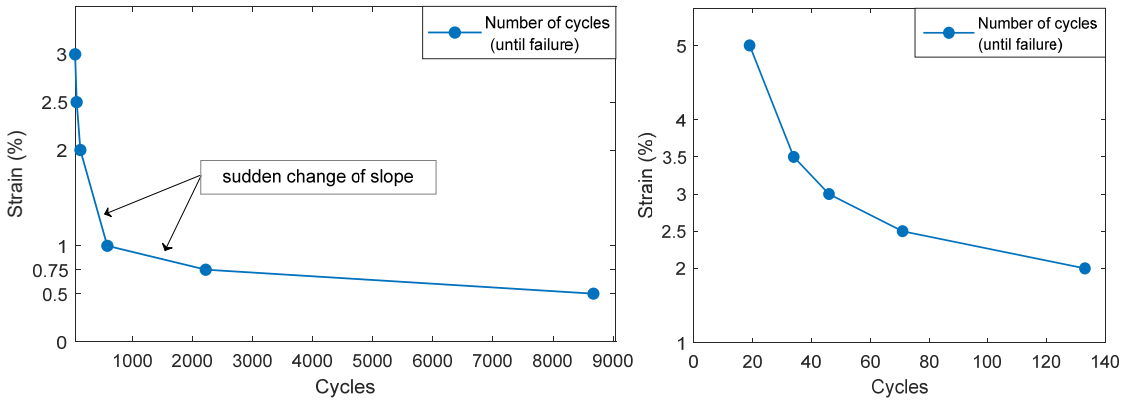


(a) (b)

Figure 8: cycles reached in different strain amplitudes

A significant variation in slope from values with <±1% strain amplitude was also observed, since the total number of cycles from ±0.75% and ±5% were greater than 1000 cycles and both of them could be considered as low cycle fatigue and rather than extremely low cycle fatigue.

### 3.2.3. Multiple Step test

This is another standard method to characterise low cycle fatigue in materials, which is used when there are only a few specimens available for testing. It involves the cyclic loading in ascendant amplitude strain every 10 or 2 cycles, which started in ±0.75% and ±0.5%, respectively. A specimen for each set of ascendant amplitude was used and a test for ascendant amplitude every 10 cycles was developed twice (MS-10C-1 and MS-10C-2). This test was strain-controlled through a strain gauge of 3mm. The load protocol can be seen in figure 7(b-c).

### 3.2.4. Seismic recorder test

A seismic recorder from Ica-Perú 2007 [42] was used and normalised from the maximum acceleration to +3.5% of strain. This represents an arbitrary protocol for comparison purposes.

The duration considered was from 4.81 to 19.81 seconds totalling 15.00 seconds and containing the maximum acceleration. Two types of adaptations of these signals were used: the first one was scaled to a total duration of 150 seconds at a strain rate of $1 \times 10^{-2}$ $s^{-1}$; the second one was scaled to 1500 seconds at a strain rate of $1 \times 10^{-3}$ $s^{-1}$. Figure 9 illustrates the adapted seismic registers.

The duration of 15.00 seconds was scaled until reaching the strain rate which was approximately similar to the strain rate of the companion test. Additionally, the variation of the strain rate was also tested.

In addition, two types of loading were used: a) the specimens were prestrained cyclically before executing the seismic recorder test; and b) the specimens did not have a prestrained history. This prestrained consisted of applying cycles of constant amplitude strain. Table 6 shows the tests, the strain rate and the prestrained type applied.

This test was controlled through an extensometer gauge, and additional measurements through a strain gauge were obtained.

Table 6: Values for seismic recorder test

| Specimen | Duration | Strain rate | Prestrain type |
|---|---|---|---|
| SR-V1-1 | 1500s | $1 \times 10^{-3}$ $s^{-1}$ | without prestrain |
| SR-V1-2 | 1500s | $1 \times 10^{-3}$ $s^{-1}$ | without prestrain |
| SR-V2-1 | 150s | $1 \times 10^{-2}$ $s^{-1}$ | without prestrain |
| SR-V2-2 | 150s | $1 \times 10^{-2}$ $s^{-1}$ | without prestrain |
| SR-V1-0.5 | 1500 s | $1 \times 10^{-3}$ $s^{-1}$ | 10 cycles of ±0.5% |
| SR-V2-0.5 | 150 s | $1 \times 10^{-2}$ $s^{-1}$ | 10 cycles of ±0.5% |
| SR-V1-1.0 | 1500 s | $1 \times 10^{-3}$ $s^{-1}$ | 10 cycles of ±1.0% |
| SR-V2-1.0 | 150 s | $1 \times 10^{-2}$ $s^{-1}$ | 10 cycles of ±1.0% |
| SR-V1-2.0 | 1500 s | $1 \times 10^{-3}$ $s^{-1}$ | 10 cycles of ±2.0% |
| SR-V2-2.0 | 150 s | $1 \times 10^{-2}$ $s^{-1}$ | 10 cycles of ±2.0% |
| SR-V1-10C | 1500 s | $1 \times 10^{-3}$ $s^{-1}$ | 10 cycles of 0.75 % + 10 cycles of ±1.0% |
| SR-V2-10C | 150 s | $1 \times 10^{-2}$ $s^{-1}$ | 10 cycles of 0.75 % + 10 cycles of ±1.0% |

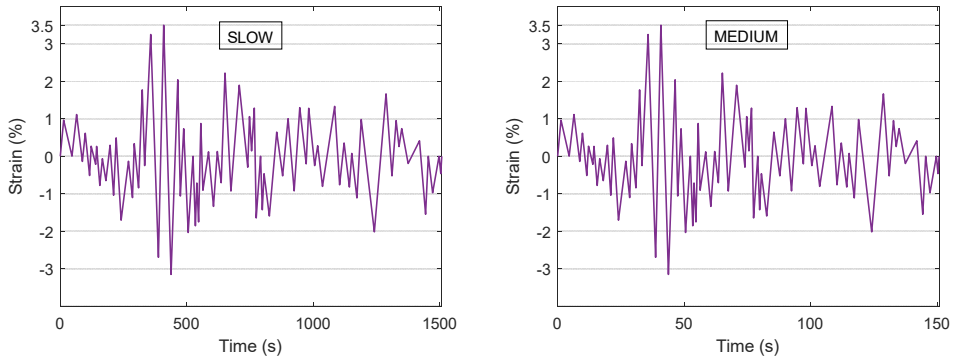


Figure 9: Seismic recorder Ica-Perú 2007 (strain normalised).

## 4. Results

### 4.1. Companion test

Table 5 shows the number of cycles reached in this test. Two stages are identified: the first one when the test was controlled by the strain gauge, and the second one when the test was controlled by the extensometer. The former was maintained until the strain gauge malfunctioned and the latter until the specimen failed.

*Stabilisation*

Stabilisation occurs when, after a certain number of developed cycles, the stress level reaches a steady-state [43] and no significant stress increment is observed in subsequent cycles. For tests ±0.75% and ±1%, strain hardening was observed, followed by a light softening, which could be considered as unstable cycles; and finally, a strain hardening until stabilisation was reached. It could be due to the martensitic transformation [44] of the stainless steel. The first hardening occurs at the first and second cycles, and the second hardening starts around the 50th and 20th cycle for ±0.75% and ±1.0% strain amplitudes, respectively.

Figures 10(a) shows the variation of maximum stress in every subsequent cycle from tests of ±0.5%, ±0.75% and ±1.0% strain amplitudes. This variation is negative, i.e. less than zero for ±0.5% tests, which means a decrease of the maximum stress in each cycle. For ±0.75% and ±1.0% strain amplitudes, the variation starts with a high increase followed by a decrease of the maximum stress (negative values) and finally the values became positive, which represent an increase of the maximum stress at an elevated number of cycles as well. However, for ±0.5% strain amplitude, a short decrease of the maximum stress was observed (figure 10(a)), which could be defined as cyclic strain softening.

In amplitudes greater than ±1%, strain hardening is clearly observed and stabilisation was considered after around 45, 20, 10 and 8 cycles for ±2.0%, ±2.5%, ±3%, and ±3.5% strain amplitudes, respectively. In some cases, such as strain amplitudes of ±4% and ±5%, the specimen fractured due to the detachment of the strain gauge, therefore not reaching stabilisation; however, one test controlled by an extensometer was developed for ±5% strain amplitude and its results were taken into account. Figure 10(b) shows the variation of maximum stress in cycles from tests of ±1.0%, ±2.0%, ±2.5%, ±3.0%, ±3.5%, and ±5.0% strain amplitudes. These variations are always positive, which means an increase of the maximum stress during cyclic loading. In addition, figure 11 shows the hysteresis loop from ±2.0% (figure 11(a)) and ±3.0% (figure 11(b)) and the strain hardening is clearly observed. Therefore, for ±2.0%, ±2.5%, ±3.0%, ±3.5%, ±4.0% and ±5.0% strain amplitudes, the strain hardening is evident since the first cycles.

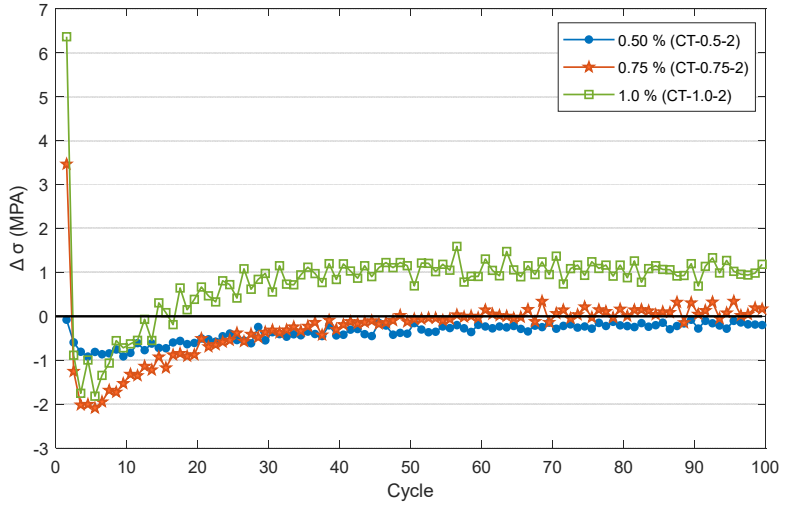


311

312 (a)

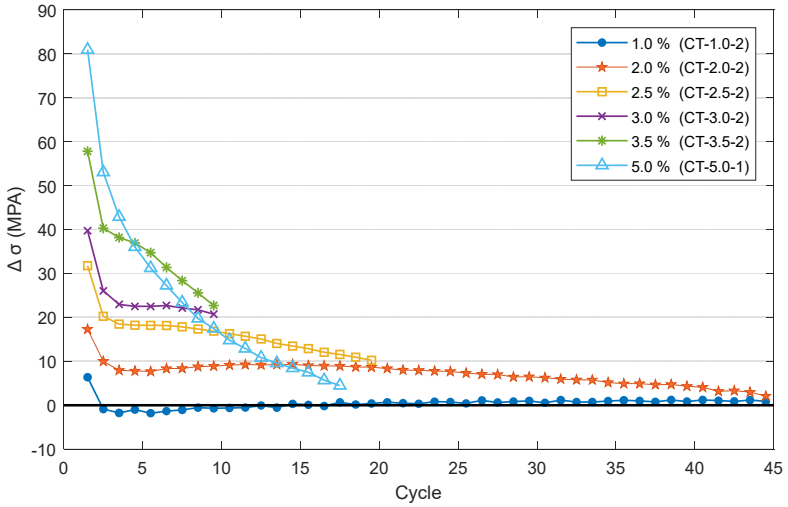


313

314 (b)

315 Figure 10: Variation of maximum stress

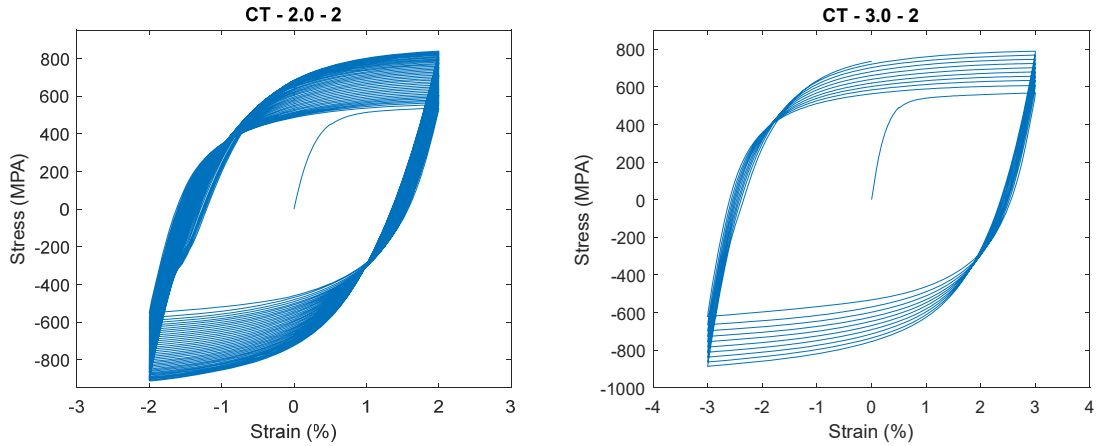


316

317 (a) (b)

318 Figure 11: Hysteresis loops

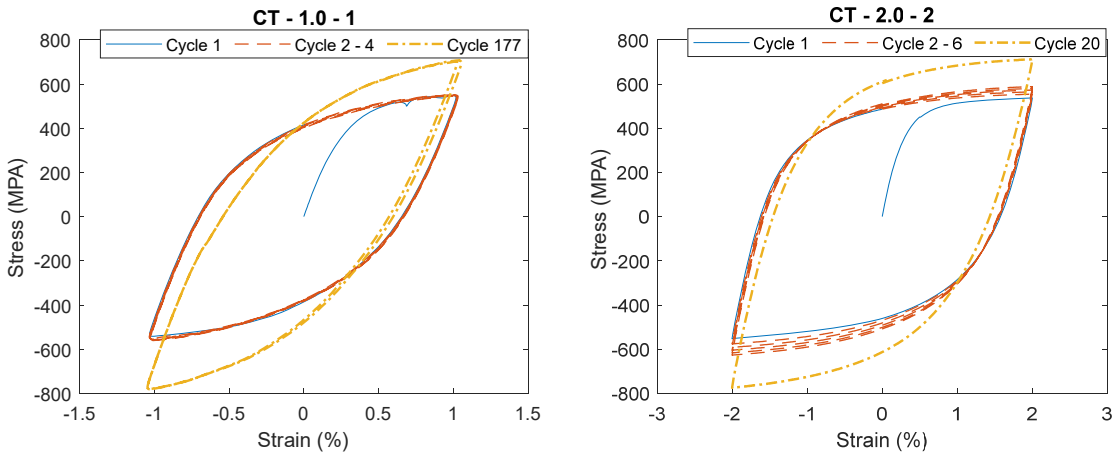


(a) (b)

Figure 12: Firsts and last hysteresis loops

Besides, figure 12(a-b) shows the difference between initial and last hysteresis loops from ±1% and ±2% strain amplitude respectively (data obtained from strain gauge). In both cases, the stress increases significantly in cycles 177 and 20, respectively, and the strain hardening is evident. In addition, in both cases, the stabilised hysteresis loop (cycle 177 and 20 for ±1% and ±2% strain amplitude) becomes narrower i.e. there is a little loss in ductility.

Furthermore, a slight change in the slope of the curve can be seen. These features are similar for ±2.5%, ±3%, ±3.5%, ±4% and ±5% strain amplitudes.

*Degradation*

In the first stage of tests with strain amplitudes equal to or less than ±1%, a pinching effect [45] was observed after approximately 1800, 400 and 200 cycles for ±0.5%, ±0.75% and ±1.0% strain amplitudes respectively, which could be attributed to a degradation of the material. In figure 13, the start of the degradation can be seen. It should be noted that after the degradation was reached, the test stopped without any apparent damage.

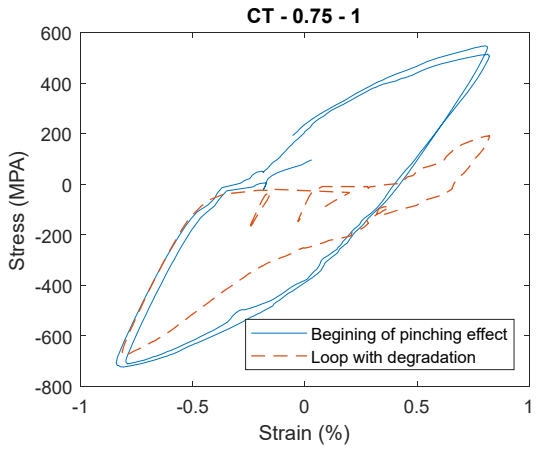


Figure 13: Degradation of the material

*Failure*

Fracture and buckling, which were considered as the end of the test, were observed after a certain number of cycles. In specimens with any apparent damage, the test was developed until it reached the fatigue fracture (controlled by extensometer) in which high elongation was not observed in all cases. However,

with amplitudes of ±1%, ±2.5% and ±3%, there was an inevitable buckling in a possibly degraded material. Figure 14 shows the final state of the specimens and the difference between the fracture from the monotonic test and low cycle fatigue.

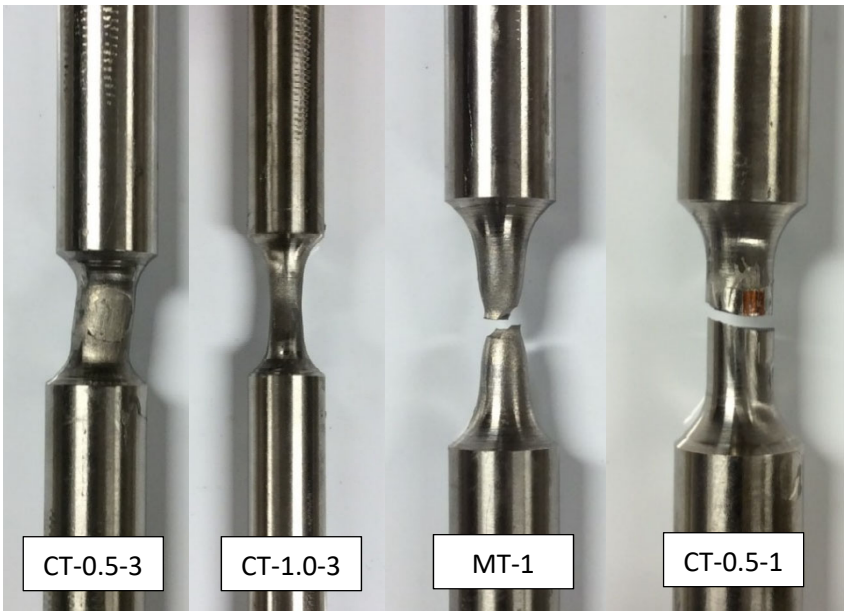


(a) (b) (c) (d)

Figure 14: Final state of specimens. (a) Buckling, (b) Necking, (c) Fracture from the monotonic test, (d) Fracture from low cycle fatigue

*The Masing Model*

A Masing material is defined as one for which the hysteresis loops of various strain ranges from a certain material coincide when their compressive peaks overlap in a common origin. It can be seen in more detail in reference [46].

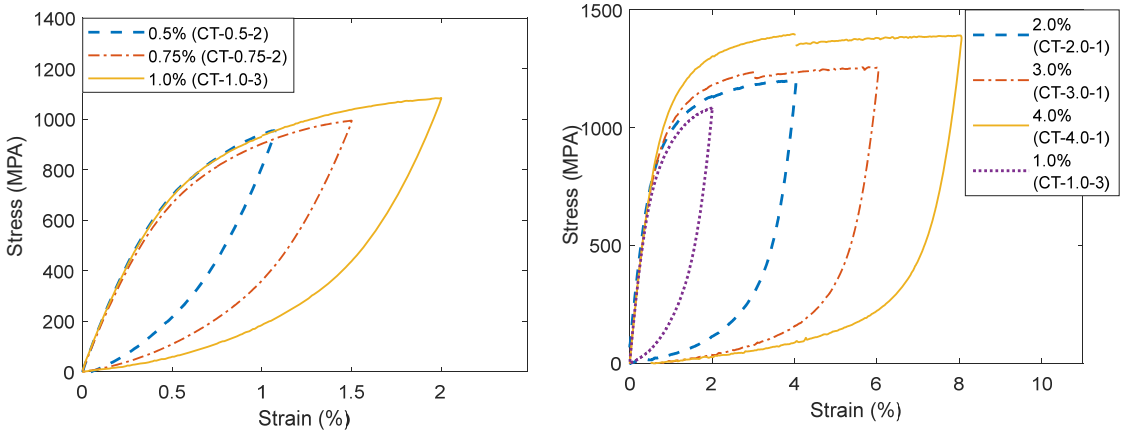


(a) (b)

Figure 15: (a) Masing from ±0.5%, ±0.75% and ±1% strain amplitudes (relative hysteresis loops); (b) Hysteresis loops in relative coordinates from ±2.0%, ±3.0% and ±4.0%

Furthermore, this behaviour in stainless steel was studied by [47][48] and found that for small strain ranges (< ±1.5%), the material was shown as "Masing material". However, for high strain ranges, stainless steel was a "no-Masing material" and this could be due to the variation of its microstructure.

This behaviour was observed in tests with strain amplitudes of ±0.5%, ±0.75% and ±1% (figure 15a) whereas the remaining ones did not show this effect (figure 15b).

Figure 15a illustrates hysteresis loops drawn in a system of relative coordinates where the Masing model can be seen. It should be noted that the first cycles of hysteresis loops were compared before specimens reached the maximum stress in the established cycle.

Finally, figure 16 shows a comparison between cyclic and monotonic stress-strain curves, where the hardening is clearly observed.

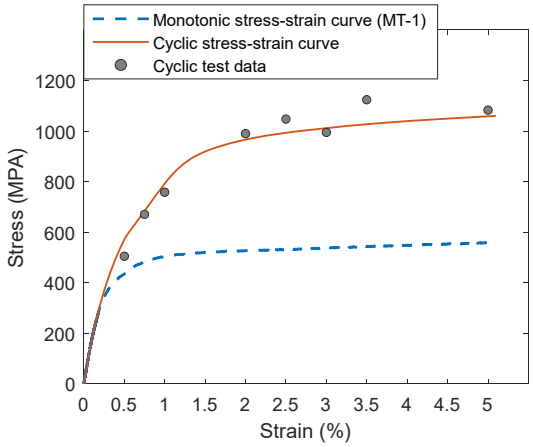


Figure 16: Comparison of cyclic and monotonic stress-strain curves stainless steel EN.1.4307

## 4.2. Multiple step

The results obtained in these tests are indicated herein as a comparison of the stress peak of every test developed.

For tests with ascendant strain amplitudes every 10 cycles, all specimens fractured after these 10 cycles reached ± 2% strain amplitude. When the ascendant strain amplitudes were every 2 cycles, the specimen fractured in ± 3% strain amplitude. In both cases, the fracture was due to the detachment of the strain gauge. Figure 17 shows hysteresis loops for both every 10 (figure 17a) and 2 cycles (figure 17b) developed.

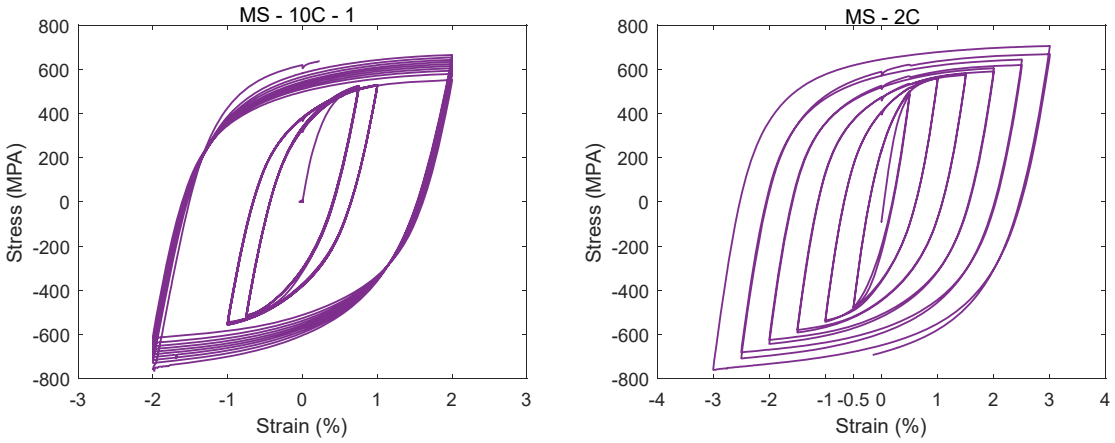


(a) (b)

Figure 17: Hysteresis loops from multiple step, (a) every 10 cycles, (b)every 2 cycles

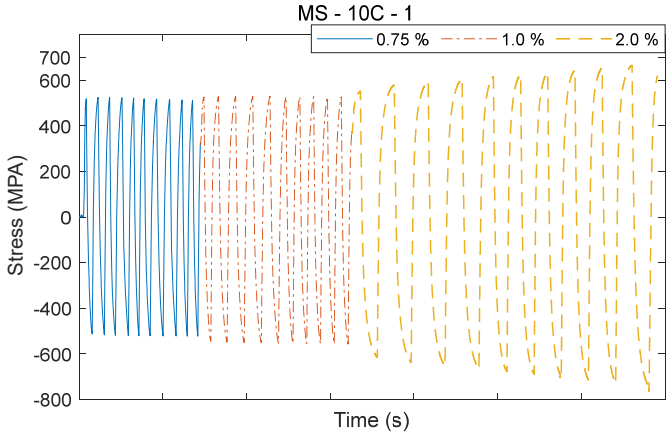


(a)

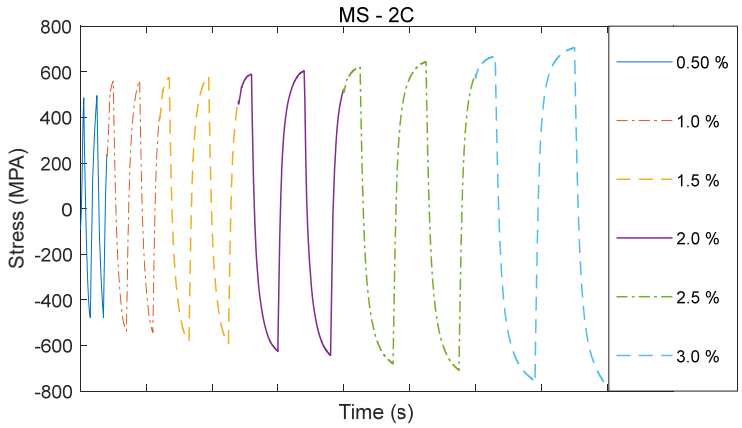


(b)

Figure 18: Maximum stress for multiple step test (every 2 cycles)

In figures 18(a) and (b), maximum stress can be seen in both cases. It was noted that maximum stress from MS-10C-1 (specimen with ascendant strain amplitude every 10 cycles) of ± 1% strain amplitude was lower than MS-2C (specimen with ascendant strain amplitude every 2 cycles). When the strain amplitude was ± 2%, the maximum stress from MS-10C-1 was higher than MS-2C.

Table 7: Maximum stress for multiple step test

| Every 2 cycles | Maximum stress (MPA) |
|---|---|
| ±0.5% | 494.80 |
| ±1.0% | 561.65 |
| ±1.5% | 580.15 |
| ±2.0% | 604.08 |
| ±2.5% | 643.80 |
| ±3.0% | 705.84 |

| Every 10 cycles | Maximum stress (MPA) |
|---|---|
| ±0.75% | 525.01 |
| ±1.0% | 529.28 |
| ±2.0% | 665.06 |

Table 7 shows the values of maximum stress. These results are consistent with the ones obtained from the Companion test since a first strain hardening from the start of the test to the second cycle was observed in strain amplitudes lower than ± 1%, continued by a softening.

## 4.3. Seismic recorder

The results of this type of tests are important for assessing non-constant strain amplitudes and high amplitudes in a short time. The maximum stress in cases both with and without prestrain are presented. Figure 19 depicts a hysteresis loop from the first 70 seconds of the SR-V2-1 (without prestrain) and SR-V2-2.0 (prestrained) tests. The stress proved to be higher in SR-V2-2.0 than SR-V2-1 due to the strain hardening developed in the prestrained specimen.

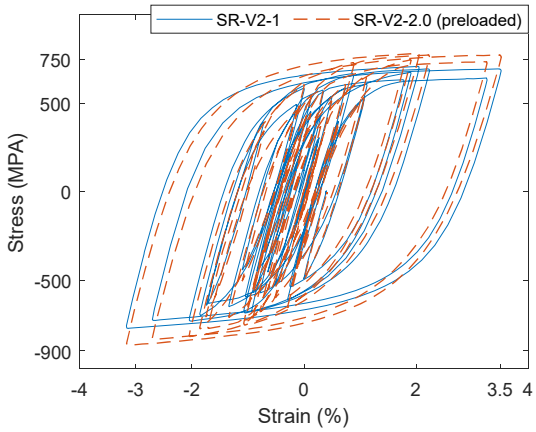


Figure 19: Hysteresis loop from first 70 seconds of seismic recorder for specimens without and with prestrain.

Table 8 depicts the maximum stress in every case and the moment when this occurs. It was at 436 s and 60 s when the duration was 1500 s and 150 s, respectively. The specimen SR-V1-1 fractured approximately at 300 s; therefore, its maximum stress was discarded.

Table 8: Maximum stress from seismic recorder

| **1500 s at strain rate of $1x10^{-3}$ $s^{-1}$** | | |
|---|---|---|
| **Specimen** | **Maximum stress (MPA)** | **Time when stress peak occurs (s)** |
| SR-V1-1 | - | - |
| SR-V1-2 | 720.73 | 436.16 |
| SR-V1-0.5 | 708.76 | 436.19 |
| SR-V1-1.0 | 675.29 | 436.24 |
| SR-V1-2.0 | 733.3 | 436.25 |
| SR-V1-10C | 700.45 | 436.23 |

| **150 s at strain rate of $1x10^{-2}$ $s^{-1}$** | | |
|---|---|---|
| **Specimen** | **Maximum stress (MPA)** | **Time when stress peak occurs (s)** |
| SR-V2-1 | 708.61 | 59.85 |
| SR-V2-2 | 654.62 | 59.86 |
| SR-V2-0.5 | 666.94 | 59.87 |
| SR-V2-1.0 | 672.09 | 59.87 |
| SR-V2-2.0 | 782.5 | 59.86 |
| SR-V2-10C | 681.96 | 59.87 |

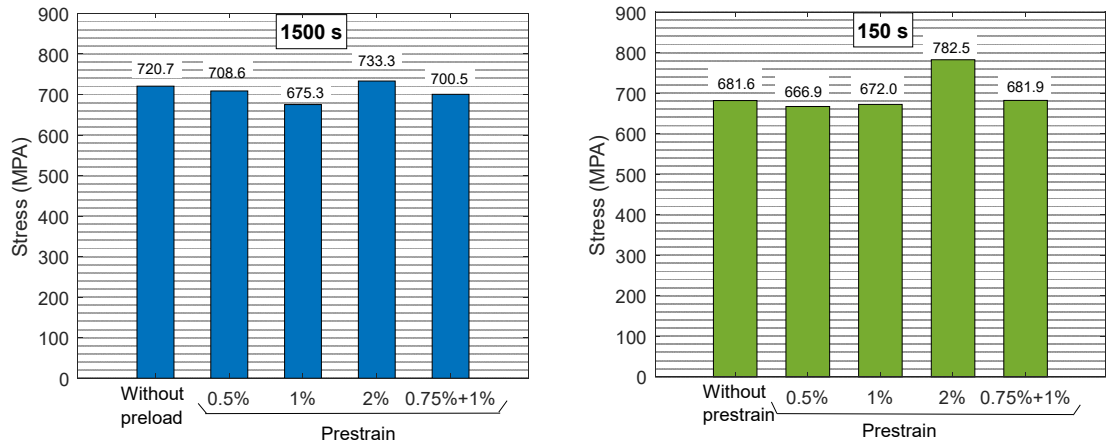


Figure 20: Maximum stress from seismic recorder

Figure 20 shows the difference between maximum stress from tests with and without prestrain (for 150 s and 1500 s of duration), and a decrease of maximum stress can be noted in all cases with history loading except when the specimen was subjected to a prestrain of ±2.0% strain amplitude. In the latter case, the maximum stress was higher with prestrain than without prestrain, i.e. the material was stronger.

These results again seem to confirm the ones obtained in the Companion test: a first strain hardening in one and two cycles followed by a softening since specimens with a minor or equal to ±1% strain amplitude prestrain showed lower maximum stress than the ones without any prestrain.

As the prestrain in all cases was 10 cycles of constant strain amplitude, the prestrain of strain amplitudes of ±0.5% and ±1.0%, specimens showed softening and therefore, maximum stress decreased. In addition, for a prestrain of ±2.0% of strain amplitude, specimens had a visible strain hardening, resulting in an increase in the maximum stress

Additionally, for all cases, the maximum stress was higher, the longer the duration, i.e. tests which lasted 1500 seconds (strain rate of 1x10-3 s-1) showed more stress than the ones at 150 seconds (strain rate of 1x10-2 s-1). One exception was observed when the specimen had a prestrain of ±2.0% strain amplitude. In this case, the maximum stress was lower, the longer the duration (1500 seconds versus 150 seconds). In conclusion, the stress was higher when the strain rate was lower, except for specimens with a prestrain of ±2% of strain amplitude.

The results of the effect of the loading history reveal important aspects to consider in seismic design (for dissipative zones) since a building could undergo other occurrences before a considerable seismic event, and worth it more research in this aspect.

### 4.4. Discussion of experimental results

In this section, the main discussion points are presented:

- For ±0.5% strain amplitudes, the strain hardening parameters were not found because, throughout all the tests, softening was observed.
- For ±0.75% and ±1% strain amplitudes, we observed a first strain hardening followed by a short softening and finally, a second strain hardening until reaching the low cycle fatigue fracture. Thus, the strain hardening parameters were obtained from the second state of strain hardening.
- For strain amplitudes of > ±1%, strain hardening was noted from the first cycles. Hence the parameters were obtained since the cycles became steady.
- Regarding seismic recorder tests, an increase in the strength and an evident strain hardening were noted when the strain amplitudes from the loading history were > ±1%. However, a decrease in the strength was observed in the specimens with prestrain of <±1% strain amplitudes.

- The maximum stress was higher when the strain rate was lower, except for specimens with a prestrain of ±2% of strain amplitudes; in this case, the maximum stress was higher when the strain rate was higher.

It is worth mentioning that a considerable strain hardening was noted in tests with >±1% strain amplitudes and different load conditions before some seismic event should be considered.

## 5. Numerical reproduction of cyclic hardening

Finally, cyclic hardening is an important feature observed in stainless steel and can be harnessed as an advantage for seismic design.

This feature was observed in tests performed with strain amplitudes higher than ±1%. For the numerical model, the Chaboche model implemented in Abaqus was used; therefore, cyclic hardening was studied through isotropic and kinematic hardening components.

*Isotropic hardening*

Equations from (1) to (4) to characterise this behaviour were used. In all cases, a value of $\sigma|_0$ (initial yielding stress) equal to 0.06% of proof stress was taken into account, with a suitable fit between tests and numerical data.

It is worth noting that parameters to characterise isotropic hardening were performed for strain amplitudes > ±1% from the first cycle to the stabilised cycle, and strain amplitudes of ±0.75% and ±1% from the second strain hardening to the stabilised cycle (since others yielded softening).

*Kinematic hardening*

Equations (5), (6), and (7) were used herein. In all cases, the parameters to characterise kinematic hardening from a stabilised cycle were obtained.

For ±0.5% strain amplitudes, parameters of strain hardening were not found because these tests showed a little softening without reaching any strain hardening.

Table 9 depicts values of strain hardening and cyclic behaviour of austenitic stainless steel. Values shown in table 10 are the ones averaged from table 8 and can be used to characterise the cyclic behaviour.

In some cases, values like CT-0.75-3, CT-1.0-3 and CT-4.0-1 were discarded due to their high scatter.

CT-5.0-1 had detached from the strain gauge in the first cycle, therefore, parameters could not be obtained.

Table 9: values of strain hardening and cyclic behaviour of austenitic stainless steel EN 1.4307

| **Specimen** | **Amplitude** | **Combined hardening parameters** | | | | |
|---|---|---|---|---|---|---|
| | | **σ0** (MPA) | **b** | **Q∞** (MPA) | **Ck** (MPA) | **γk** |
| CT-0.75-1 | ±0.75% | 378 | 0.32 | 70 | 77270 | 70 |
| CT-0.75-2 | ±0.75% | 355 | 0.64 | 12 | 86090 | 180 |
| CT-1.0-1 | ±1% | 373 | 0.22 | 138 | 54597 | 310 |
| CT-1.0-2 | ±1% | 363 | 0.33 | 63 | 58647 | 304 |
| CT-1.0-3 | ±1% | 354 | 0.18 | 102 | 59596 | 310 |
| CT-2.0-1 | ±2.0% | 357 | 0.78 | 155 | 55750 | 227 |
| CT-2.0-2 | ±2.0% | 310 | 0.77 | 120 | 62720 | 224 |
| CT-2.5-1 | ±2.5% | 343 | 1.06 | 116 | 62450 | 214 |
| CT-2.5-2 | ±2.5% | 351 | 1.04 | 148 | 41050 | 215 |
| CT-3.0-1 | ±3% | 356 | 1.64 | 169 | 41680 | 199 |
| CT-3.0-2 | ±3% | 348 | 2.24 | 85 | 51610 | 182 |
| CT-3.5-1 | ±3.5% | 302 | 2.33 | 112 | 41900 | 175 |

| | | | | | | |
|---|---|---|---|---|---|---|
| CT-3.5-2 | ±3.5% | 337 | 1.92 | 109 | 58450 | 186 |
| CT-4.0-1 | ±4% | 349 | 14.08 | 83 | 33510 | 175 |
| CT-4.0-2 | ±4% | 362 | 5.12 | 63 | 39500 | 157 |
| CT-5.0-1 | ±5% | - | - | - | - | - |
| CT-5.0-2 | ±5% | 419 | 0.83 | 149 | 47692 | 131 |

Table 10: Proposed values to characterise cyclic behaviour of austenitic stainless steel EN 1.4307 (average)

| **Amplitude** | **Combined hardening parameters** | | | | |
|---|---|---|---|---|---|
| | **σ0** (MPA) | **b** | **Q∞** (MPA) | **Ck** (MPA) | **γk** |
| ±0.75% | 367 | 0.48 | 41 | 81680 | 125 |
| ±1% | 368 | 0.28 | 101 | 56622 | 307 |
| ±2.0% | 334 | 0.78 | 137.05 | 59235 | 226 |
| ±2.5% | 347 | 1.05 | 132 | 51750 | 215 |
| ±3% | 352 | 1.94 | 127 | 46645 | 191 |
| ±3.5% | 320 | 2.13 | 110 | 50175 | 181 |
| ±4% | 362 | 5.12 | 63 | 39500 | 157 |
| ±5% | 419 | 0.83 | 149 | 47692 | 131 |

## 6. Conclusions

The main aim of this research was the characterisation of austenitic stainless steel EN 1.4307 to understand the cyclic behaviour and low cycle fatigue for seismic use purposes when intended for dissipative zones. This study conducted a set of tests of 37 specimens subjected to several regular and arbitrary loading protocols. The conclusions of this study are as follows:

- Hardening was observed in most of the specimens, i.e. ±0.75%, ±1%, ±2%, ±2.5%, ±3%, ±3.5%, ±4%, ±5%. The greater the applied total strain amplitudes, the higher the strain hardening could be demonstrated
- The standard protocol methods developed showed consistent results.
- Using experimental results, values of interest for analytical models of stainless steel EN 1.4307 subject to cyclic loading were obtained ($Q_\infty$, $b$, $C_k$, $\gamma_k$).
- Arbitrary protocol from a seismic recorder was carried out and specimens with prestrain higher than ±1% cyclic strain amplitudes reached a high level of stress.
- Our experimental results, which were at the material level, proved that the hardening was dependent on the load history. To assess the use of this material in dissipative zones of buildings, further studies at a structural level, which take the load history of the assessed structure into account, are needed.

**Acknowledgements**

The authors acknowledge the financial support provided by the Project BIA2016-75678-R, AEI/FEDER, UE "*Comportamiento estructural de pórticos de acero inoxidable. Seguridad frente a acciones accidentales de sismo y fuego*", funded by the Spanish Ministry of Economic Affairs and Digital Transformation (MINECO). The first author acknowledges the financial support from the Peruvian Government *Beca Generación del Bicentenario*.

## References

[1] I. Arrayago, E. Real, and L. Gardner, “Description of stress-strain curves for stainless steel alloys,” *Mater. Des.*, vol. 87, pp. 540–552, 2015.

[2] K. J. R. Rasmussen, “Full-range stress-strain curves for stainless steel alloys,” *Res. Rep. - Univ. Sydney, Dep. Civ. Eng.*, vol. 59, no. 811, pp. 1–44, 2001.

[3] E. Mirambell and E. Real, “On the calculation of deflections in structural stainless steel beams: An experimental and numerical investigation,” *J. Constr. Steel Res.*, vol. 54, no. 1, pp. 109–133, 2000.

[4] M. J. Joseph and M. A. Jabbar, “Effect of aging process on the microstructure, corrosion resistance and mechanical properties of stainless steel AISI 204,” *Case Stud. Constr. Mater.*, vol. 11, p. e00253, 2019.

[5] X. Wu, L. Li, H. Li, B. Li, and Z. Ling, “Effect of strain level on corrosion of stainless steel bar,” *Constr. Build. Mater.*, vol. 163, pp. 189–199, 2018.

[6] L. Li, C. F. Dong, K. Xiao, J. Z. Yao, and X. G. Li, “Effect of pH on pitting corrosion of stainless steel welds in alkaline salt water,” *Constr. Build. Mater.*, vol. 68, pp. 709–715, 2014.

[7] I. Arrayago, I. González-de-León, E. Real, and E. Mirambell, “Tests on stainless steel frames. Part I: Preliminary tests and experimental set-up,” *Thin-Walled Struct.*, vol. 157, 2020.

[8] I. Arrayago, I. González-de-León, E. Real, and E. Mirambell, “Tests on stainless steel frames. Part II: Results and analysis,” *Thin-Walled Struct.*, vol. 157, 2020.

[9] F. Walport, M. Kukukler and L. Gardner. "Stability Design of Stainless Steel Structures". *Journal of Structural Engineering*. Vol. 148(1).

[10] I. Arrayago, E. Real, E. Mirambell, and R. Chacón, “12.01: Global plastic design of stainless steel frames,” *Ce/Papers*, vol. 1, no. 2–3, pp. 3463–3471, 2017.

[11] Y. Shen and R. Chacón, “Geometrically non-linear analysis with stiffness reduction for the stability design of stainless steel structures: Application to members and planar frames,” *Thin-Walled Struct.*, vol. 148, no. July 2019, 2020.

[12] Y. Shen and R. Chacón, “Flexural stiffness reduction for stainless steel SHS and RHS members prone to local buckling,” *Thin-Walled Struct.*, vol. 155, no. March, 2020.

[13] F. Walport, L. Gardner, E. Real, I. Arrayago, and D. A. Nethercot, “Effects of material nonlinearity on the global analysis and stability of stainless steel frames,” *J. Constr. Steel Res.*, vol. 152, pp. 173–182, 2019.

[14] F. Walport, L. Gardner, and D. A. Nethercot, “Design of structural stainless steel members by second order inelastic analysis with CSM strain limits,” *Thin-Walled Struct.*, vol. 159, no. October 2020, p. 107267, 2021.

[15] R. Chacón, A. Vega, and E. Mirambell, “Numerical study on stainless steel I-shaped links on eccentrically braced frames,” *J. Constr. Steel Res.*, vol. 159, pp. 67–80, 2019.

[16] J. D. Gao, X. X. Du, H. X. Yuan, and M. Theofanous, “Hysteretic performance of stainless steel double extended end-plate beam-to-column joints subject to cyclic loading,” *Thin-Walled Struct.*, vol. 164, no. March, 2021.

[17] J. L. Chaboche, “A review of some plasticity and viscoplasticity constitutive theories,” *Int. J. Plast.*, vol. 24, no. 10, pp. 1642–1693, 2008.

[18] W. Zhang *et al.*, “Characterization of the cyclic softening and remaining creep behaviour of P92 steel weldment,” *J. Mater. Res. Technol.*, vol. 15, pp. 1446–1456, 2021.

[19] T. S. Srivatsan, M. Al-Hajri, and V. K. Vasudevan, “Cyclic plastic strain response and fracture behavior of 2009 aluminum alloy metal-matrix composite,” *Int. J. Fatigue*, vol. 27, no. 4, pp. 357–371, 2005.

[20] C. Wang, L. yan Xu, and J. sheng Fan, “Cyclic softening behavior of structural steel with strain range dependence,” *J. Constr. Steel Res.*, vol. 181, p. 106658, 2021.

[21] Q. He, Y. Chen, K. Ke, M. C. H. Yam, and W. Wang, “Experiment and constitutive modeling on cyclic

plasticity behavior of LYP100 under large strain range," *Constr. Build. Mater.*, vol. 202, pp. 507–521, 2019.

[22] A. A. Fernandes, A. M. P. de Jesus, and R. N. Jorge, *Monotonic and ultra-low-cycle fatigue behaviour of pipeline steels: Experimental and numerical approaches*. 2018.

[23] K. H. Nip, L. Gardner, C. M. Davies, and A. Y. Elghazouli, "Extremely low cycle fatigue tests on structural carbon steel and stainless steel," *J. Constr. Steel Res.*, vol. 66, no. 1, pp. 96–110, 2010.

[24] A. Dutta, S. Dhar, and S. K. Acharyya, "Material characterization of SS 316 in low-cycle fatigue loading," *J. Mater. Sci.*, 2010.

[25] S. Chandra, S. Goyal, R. Sandhya, and S. K. Ray, "Low cycle fatigue life prediction of 316 L ( N ) stainless steel based on cyclic elasto-plastic response," *Nucl. Eng. Des.*, vol. 253, pp. 219–225, 2012.

[26] Y. Q. Wang, T. Chang, Y. J. Shi, H. X. Yuan, L. Yang, and D. F. Liao, "Thin-Walled Structures Experimental study on the constitutive relation of austenitic stainless steel S31608 under monotonic and cyclic loading," *Thin Walled Struct.*, vol. 83, pp. 19–27, 2014.

[27] R. A. Chacon, M. D. De Marco, E. Real, and I. Arrayago, "Experimental Study on the Cyclic Response of Austenitic Stainless Steel," *International Conference on Advances in Steel Structures* December, Hong Kong, 2018.

[28] X. Chang, L. Yang, L. Zong, M. H. Zhao, and F. Yin, "Study on Cyclic Constitutive Model and Ultra Low Cycle Fracture Prediction Model of Duplex Stainless Steel," *J. Constr. Steel Res.*, vol. 152, pp. 105–116, 2019.

[29] M. Baiguera, G. Vasdravellis, and T. L. Karavasilis, "Ultralow Cycle Fatigue Tests and Fracture Prediction Models for Duplex Stainless-Steel Devices of High Seismic Performance Braced Frames," *J. Struct. Eng.*, vol. 145, no. 1, pp. 1–18, 2019.

[30] F. Yin, L. Yang, M. Wang, L. Zong, and X. Chang, "Study on ultra-low cycle fatigue behavior of austenitic stainless steel," *Thin-Walled Struct.*, vol. 143, p. 106205, 2019.

[31] A. Charles-Darwin and E. Beaumont, "Low-cycle fatigue of stainless steel plates under large plastic strain demands," *J. Build. Eng.*, vol. 29, no. July 2019, p. 101160, 2020.

[32] A. American and N. Standard, "Seismic Provisions for Structural Steel Buildings," 2016.

[33] H. Stephens, R., Fatemi, A., Stephens, R., Fuchs, *Metal Fatigue in Engineering*. 2000.

[34] Z. Xie and Y. Chen, "Experimental and modeling study of uniaxial cyclic behaviors of structural steel under ascending/descending strain amplitude-controlled loading," *Constr. Build. Mater.*, vol. 278, p. 122276, 2021.

[35] S. Chandra Roy, S. Goyal, R. Sandhya, and S. K. Ray, "Analysis of Hysteresis Loop of 316L(N) Stainless Steel under Low Cycle Fatigue Loading Conditions," *Procedia Eng.*, vol. 55, pp. 165–170, 2013.

[36] S. Jia, Q. Tan, J. Ye, Z. Zhu, and Z. Jiang, "Experiments on dynamic mechanical properties of austenitic stainless steel S30408 and S31608," *J. Constr. Steel Res.*, vol. 179, p. 106556, 2021.

[37] A. (2012). E606/E606M., "Standard test method for stain-controlled fatigue testing." .

[38] R. Manual, "Instron Load Frames Reference Manual - Pre-Installatio n © Copyright 2001 Instron Corporation."

[39] Tokyo Measuring Instruments Lab., "General use strain gauge." [Online]. Available: https://tml.jp/eng/documents/strain_gauge/Fseries.pdf.

[40] Y. Huang and B. Young, "The art of coupon tests," *J. Constr. Steel Res.*, vol. 96, pp. 159–175, 2014.

[41] W. Ramberg, W., & Osgood, "Description of stress-strain curves by three parameters," *USA Natl. Advis. Comm. Aeronaut. Note No. 902*, 1943.

[42] Instituto Geofísico del Perú, "Sismo de Pisco del 15 de Agosto, 2007 (7.9Mw) Departamento de Ica - Perú (Informe preliminar)," 2007. [Online]. Available:

https://repositorio.igp.gob.pe/handle/20.500.12816/1115.

[43] H. Krawinkler, H., Zohrei, M., Lashkari-Irvani, B., Cofie, N. and Hadidi-Tamjed, *Recommendations for Experimental Studies on the Seismic Behavior of Steel Components and Materials*, Report 61. 1983.

[44] Y. Li, D. Yu, B. Li, and X. Chen, "Martensitic transformation of an austenitic stainless steel under non- proportional cyclic loading," *Int. J. Fatigue*, vol. 124, no. February, pp. 338–347, 2019.

[45] FEMA P440A, *Effects of Strength and Stiffness Degradation on Seismic Response*. 2009.

[46] R. P. Skelton, H. J. Maier, and H. J. Christ, "The Bauschinger effect, Masing model and the Ramberg-Osgood relation for cyclic deformation in metals," *Mater. Sci. Eng. A*, vol. 238, no. 2, pp. 377–390, 1997.

[47] F. Zhou and L. Li, "Experimental study on hysteretic behavior of structural stainless steels under cyclic loading," *J. Constr. Steel Res.*, vol. 122, pp. 94–109, 2016.

[48] S. Sivaprasad, S. K. Paul, N. Narasaiah, and S. Tarafder, "Experimental investigation on cyclic deformation behaviour of primary heat transport piping materials: Masing analysis of hysteresis loops," *Trans. Indian Inst. Met.*, vol. 63, no. 2–3, pp. 559–563, 2010.